Main Rotor–Tail Rotor Interaction and Its Implications for Helicopter Directional Control

Timothy M. Fletcher
Postgraduate Research Student
Department of Aeronautics
Imperial College, London, UK

Richard E. Brown*
Mechan Chair of Engineering
Department of Aerospace Engineering
University of Glasgow, Glasgow, UK

Aerodynamic interference between the main and tail rotor can have a strong negative influence on the flight mechanics of a conventional helicopter. Significant unsteadiness in the tail rotor loading is encountered under certain flight conditions, but the character of the unsteadiness can depend on the direction of rotation of the tail rotor. Numerical simulations, using Brown's vorticity transport model, of the aerodynamic interaction between the main and tail rotors of a helicopter are presented for a range of forward and lateral flight trajectories. Distinct differences are predicted in the behavior of the system in left and right sideward flight that are consistent with flight experience that the greatest fluctuations in loading or control input are required in left sideways flight (for a counterclockwise rotating main rotor). These fluctuations are generally more extreme for a system with tail rotor rotating top-forward than top-aft. Differences are also exposed in the character of the lateral excitation of the system as forward flight speed is varied. The observed behavior appears to originate in the disruption of the tail rotor wake that is induced by its entrainment into the wake of the main rotor. The extent of the disruption is dependent on flight condition, and the unsteadiness of the process depends on the direction of rotation of the tail rotor. In intermediate-speed forward flight and right sideward flight, the free stream delays the entrainment of the tail rotor wake far enough downstream for the perturbations to the rotor loading to be slight. Conversely, in left sideward and quartering flight, the free stream confines the entrainment process close to the rotors, where it causes significant unsteadiness in the loads produced by the system.

Nomenclature

$C_{T_{\mathrm{tr}}}$ tail rotor thrust coefficient, $T_{\mathrm{tr}}/\rho A(\Omega_{\mathrm{tr}}R_{\mathrm{tr}})^2$
F current airframe forces and moments
F^* target airframe forces and moments
i sample index
N airframe yaw moment
N_{mr} main rotor contribution to yaw moment
N_{tr} tail rotor contribution to yaw moment
R main rotor radius
R_{tr} tail rotor radius
S vorticity source
T_{tr} tail rotor thrust
Δt time interval
u flow velocity
u_{b} flow velocity relative to blade
θ_0 main rotor collective pitch
$\theta_{0_{\mathrm{tr}}}$ tail rotor collective pitch
$\theta_{1\mathrm{c}}$ lateral cyclic pitch
$\theta_{1\mathrm{s}}$ longitudinal cyclic pitch
μ overall advance ratio, $(\mu_x^2+\mu_y^2)^{1/2}$
μ_x advance ratio in forward direction
μ_y advance ratio in lateral direction; positive to right
$\tilde{\mu}_y$ lateral advance ratio, scaled by $\frac{(\Omega_{\mathrm{tr}}R_{\mathrm{tr}})}{(\Omega R)}(C_{T_{\mathrm{tr}}}/2)^{-1/2}$
ν kinematic viscosity
τ matrix of time constants
ω vorticity
ω_{b} bound vorticity on blade
Ω main rotor speed
Ω_{tr} tail rotor speed

Notation

$\bar{x}$ time-averaged value of $x(t)$
x' perturbation of $x(t)$ from time average
$\hat{x}$ root mean square (RMS) value of $x(t)$

Introduction

The need to correct or rectify the effects of aerodynamic interactions that were unforeseen or mispredicted at the design stage has historically been one of the most common causes of delay in the advancement of a new helicopter design from prototype to production. Interference between the wakes and other flow disturbances induced by the helicopter's rotors, fuselage, and lifting surfaces can produce strong loads on geometrically distant parts of the configuration. Any unsteadiness in these loads, or change in these loads as the flight condition of the aircraft is altered,

*Corresponding author; email: r.brown@aero.gla.ac.uk.
Manuscript received January 2007; accepted October 2007.

can have a very strong negative influence on the dynamics of the vehicle. Experience within the helicopter industry suggests that the nature and form of the aerodynamic interactions that arise from even minor configurational changes to an airframe can be extremely difficult to predict, and this lack of predictive capability attaches a significant degree of risk to any departures from a successful configuration.

In a conventionally configured helicopter, a single, large main rotor provides propulsion and lift, while a smaller tail rotor, mounted behind the main rotor, is oriented transversely to the main rotor to provide a countertorque reaction to the fuselage. This paper will focus on a particularly poorly understood element of the interactional aerodynamic environment of this configuration, namely the effect on the performance of the tail rotor of its operation in close proximity to the flow field of the main rotor. The interaction of the main rotor wake with that of the tail rotor, and more directly, its impingement on the tail rotor itself, adds both unsteadiness and nonlinearity to the performance of the tail rotor.

In 1980, Sheridan and Smith (Ref. 1) produced an authoritative survey of the various known aerodynamic interactions within the helicopter system. In the interests of drawing the community's attention to the problems caused by aerodynamic interaction within the helicopter system, its many and varied manifestations were categorized according to the aircraft components involved in the interaction (e.g., "main rotor–fuselage" or "main rotor–tail rotor") and the associated flow anomaly (e.g., "flow redirection," "flow field distortion," or "wake impingement") responsible for the observed dynamic effects on the system. Indeed, Sheridan and Smith noted that thrust distortion and an increased power requirement, compared to the same rotors tested in isolation, were specific problems associated with main rotor–tail rotor interaction. Interestingly, Sheridan and Smith also categorized main rotor–tail rotor and tail rotor–main rotor interactions separately, acknowledging the effects of mutual interference on the performance of both components.

An important design parameter, from a handling qualities perspective at least, appears to be the sense of rotation of the tail rotor. The tail rotor of a conventional helicopter can be classified as having either top-aft (TA) or top-forward (TF) sense of rotation, implying that its blades travel, respectively, rearward or forward at the top of the disk. Helicopter designers often refer to a "right way" and a "wrong way" for the tail rotor to rotate, in the belief that top-aft tail rotors encounter fewer aerodynamic problems than those with top-forward rotation. Hence, a tail rotor with TA sense of rotation is usually the first choice for a new helicopter design. The overview of tail rotor design published by Lynn et al. (Ref. 2) in 1970 described clear differences in performance for systems with TA and TF rotation, but also acknowledged the obscurity of the aerodynamic origins of these differences. The differences in performance between systems equipped with TA and TF rotating tail rotors seem to manifest themselves most clearly in sideways flight as a large increase in the pedal activity required to trim the aircraft in yaw with tail rotors having TF sense of rotation usually being more susceptible to this effect than those with TA rotation. Yet the number of helicopters in the last few decades that have progressed through the design process, only to have the direction of rotation of their tail rotors reversed during full-scale development, testifies to a continued lack of understanding of the detailed reasons why the direction of tail rotor rotation should have such a marked effect on aircraft performance. Notable works describing situations where the sense of rotation of the tail rotor became a significant issue in the design of the aircraft include the study of the AH-56A Cheyenne by Johnston and Cook (Ref. 3), the YAH-64 Apache by Amer et al. (Ref. 4), and Prouty (Ref. 5), and the wind-tunnel tests by Yeager et al. (Ref. 6). In addition, it is likely that the tail shake phenomenon (Ref. 7), which has emerged during flight test of several helicopters, is also exacerbated by main rotor–tail rotor aerodynamic interaction and is influenced, to some extent, by the direction of rotation of the tail rotor.

Unfortunately, most published experimental research on main rotor–tail rotor aerodynamic interaction has been performed on configurations where it has been difficult to isolate the specific effects of the aerodynamic interaction between the main and tail rotors on the performance of the system. Inferences from the influential data obtained by Balch (Ref. 8), for instance, are obscured by the presence of a fuselage in the experimental setup. The works of Empey and Ormiston (Ref. 9) and Wiesner and Kohler (Ref. 10) were both valuable contributions to the field, but interpretation of both studies is complicated by the presence of strong ground effect.

Although much remains to be achieved, numerical helicopter models, particularly those using computational fluid dynamics (CFD) techniques to capture the structure and form of the wakes induced by helicopter rotors, have advanced to the point where the potential exists to model some aspects of the aerodynamic interactions between the various components of the helicopter to an appreciable degree of realism. The present work uses such a model to examine the flow physics that underlies the aerodynamic interaction between the main and tail rotors of the conventional helicopter configuration, and in particular to investigate some of the differences in aerodynamic behavior of the system that result from a change in the sense of rotation of the tail rotor. The advantage of the computational approach is that, unlike in the laboratory or in full-scale flight test, complicating factors such as the presence of ground effect, and the uncertainty in interpretation of results that is introduced by the presence of secondary aerodynamic interference from fuselage and fins, can be eliminated very easily, revealing the fundamental processes at work.

Helicopter Model

The performance of a generic conventional helicopter configuration has been simulated using the vorticity transport model (VTM) developed by Brown (Ref. 11), and extended by Brown and Line (Ref. 12). The VTM is a comprehensive rotorcraft model in which the flow field around the rotorcraft is obtained by solving the time-dependent Navier–Stokes equation, in finite-volume form, on a structured Cartesian mesh enclosing the helicopter system. The key feature of the VTM is its use of the vorticity–velocity form of the incompressible Navier–Stokes equation,

$$\frac{\partial}{\partial t}\omega + u \cdot \nabla\omega - \omega \cdot \nabla u = S + \nu\nabla^2\omega \tag{1}$$

that relates the evolution of the vorticity field ω, representing the wake, to the velocity field u. An adaptive grid formulation is used in which cells exist only where there is vorticity. The source term

$$S = -\frac{d}{dt}\omega_b + u_b\nabla \cdot \omega_b \tag{2}$$

accounts for the production of vorticity in the flow as a result of spatial and temporal changes in the bound vorticity distribution ω_b on the various lifting surfaces of the rotorcraft. In the current version of the VTM, the blade aerodynamics is modeled using an extension of the Weissinger-L lifting line theory. Local blade stall is modeled using a variation on Kirchoff's trailing edge separation model, where the length of the stall cell is given as a prescribed function of local angle of attack based on known airfoil characteristics. The velocity field is related to the vorticity field by using a Cartesian fast multipole method to invert the differential form of the Biot–Savart law:

$$\nabla^2 u = -\nabla \times \omega \tag{3}$$

Use of the fast multipole method in conjunction with the adaptive grid renders the approach effectively boundary free (Ref. 12). Numerical diffusion of the vorticity in the flow field surrounding the rotorcraft is kept at a very low level by using a Riemann problem technique based on Toro's

weighted average flux method (Ref. 13) to advance Eq. (1) through time. This approach allows highly efficient multirotor simulations, and permits many rotor revolutions to be captured without significant dissipation of the wake structure, in contrast to the performance of more conventional CFD techniques based on the pressure-velocity formulation of the Navier–Stokes equation. Hence, in principle, both the low (lower than 1/rev) frequency components of the loading, which influence the body dynamics but are often the result of the dynamics of large-scale structures in the flow, and the high-frequency (1/rev and higher) components, which are important for the dynamic response of the rotors but are generally governed by smaller scale flow features such as blade–vortex interactions, can be resolved simultaneously within the same computation. The VTM has been used previously for helicopter flight mechanics research by Brown and Houston (Ref. 14) and Houston and Brown (Ref. 15), for the investigation of the interaction of helicopters with aircraft wakes by Whitehouse and Brown (Ref. 16), and the rotor vortex ring state by Ahlin and Brown (Ref. 17).

In this study, the helicopter is represented simply as a pair of rotors, oriented in conventional fashion with their centers located at representative points in the flow. This idealization of the problem ensures that solely the effects of the interactions between the rotors are captured, uncomplicated by the presence of further aerodynamic interactions between rotors and fuselage or empennage. The principal parameters for the main and tail rotors are given in Tables 1 and 2, respectively, and the relative locations of the main and tail rotors are shown in Fig. 1. The main rotor rotates counterclockwise when viewed from above (the convention for American and British helicopters), hence the tail rotor produces a force to starboard in trimmed flight. All blades are assumed to be rigid and the rotors both have articulated hubs.

In all calculations, the rigid-body modes of the system were suppressed, yielding the computational equivalent of a model mounted rigidly in the test section of a wind tunnel. This was done to simplify the analysis by eliminating feedback from the rigid-body modes into the aerodynamic loads generated on the rotors. In each simulation, the main rotor collective pitch was controlled to develop a prespecified main rotor thrust coefficient. Meanwhile, the tail rotor collective pitch was controlled to ensure a zero net yaw moment on the rotorcraft, thus providing

Table 1. Main rotor data

No. of blades	3
Rotor radius	R
Chord	$0.055R$
Twist	-8° (linear)
Airfoil	NACA 0012
Root cutout	$0.19R$
Flap hinge offset	$0.0875R$
Rotational speed	Ω
Thrust coefficient, C_T	0.005

Table 2. Tail rotor data

No. of blades	3
Rotor radius	$R_{tr} = 0.193R$
Chord	$0.186R_{tr}$
Twist	0°
Airfoil	NACA 0012
Root cutout	$0.21R_{tr}$
Flap hinge offset	0.0
Rotational speed	$\Omega_{tr} = 5.25\Omega$
δ_3	45°

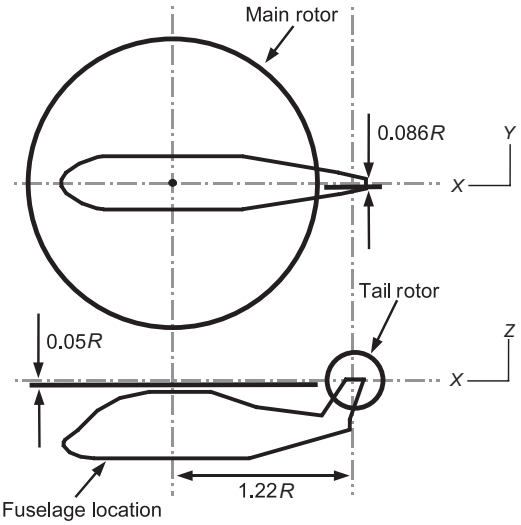

Fig. 1. Rotor configuration (fuselage represented solely for clarity).

a realistic flight condition in yaw and allowing the sensitivity of the control response to aerodynamic interaction to be evaluated. To eliminate as much complication from the analysis as possible, the longitudinal and lateral main rotor cyclic pitch was controlled to satisfy a very simplified trim condition of zero tilt of the main rotor disk, measured with respect to its shaft. The trim algorithm used within the calculations was a simple first-order scheme in which the instantaneous rate of change of the vector of controls, $u = (\theta_0, \theta_{1s}, \theta_{1c}, \theta_{0tr})$, is taken to be proportional to the error between a vector F, consisted of the forces, moments, and disk-tilt angles that are to be controlled, and a vector of specified target values F^*:

$$\tau \frac{du}{dt} = F^* - F(t) \tag{4}$$

where τ is a suitably defined matrix of time constants. Use of this controller yields an element of subjectivity in any measurements of control activity, since the results are affected by the particular choice of the elements of τ. These elements were thus set to prevent significant control input at frequencies much above 0.2–0.4 per main rotor revolution (as shown in Fig. 2), and hence to be roughly representative of the capabilities of a human pilot. Note though that this approach to the control of the helicopter needs to be tempered by the fact that, in handling qualities terms, the pilot is able to apply control inputs with a variety of different levels of aggression, the actual level depending on the task at hand. In general, the pilot will compromise on a certain degree of variability in the trajectory of the aircraft in exchange for a relaxation in required control activity. The results presented here thus fit within a broader spectrum of data that might be obtained by considering a more complete range of pilot attributes.

If the dynamics of the system is to be captured convincingly across the entire frequency spectrum of interest, then each simulation needs to be run for a very large number of rotor revolutions. The effort required to capture especially the low-frequency dynamics of the system results in simulations that are particularly demanding in terms of both memory and computational time. Thus, it is important to find a practical balance between computational effort and adequate resolution of the physical effects of importance in the situation being modeled. Figure 2 shows part of the Fourier spectrum of the variation of tail rotor collective required to trim the helicopter in yaw in a series of test computations with the flow around the rotors resolved by grids with various cell sizes. The quartering

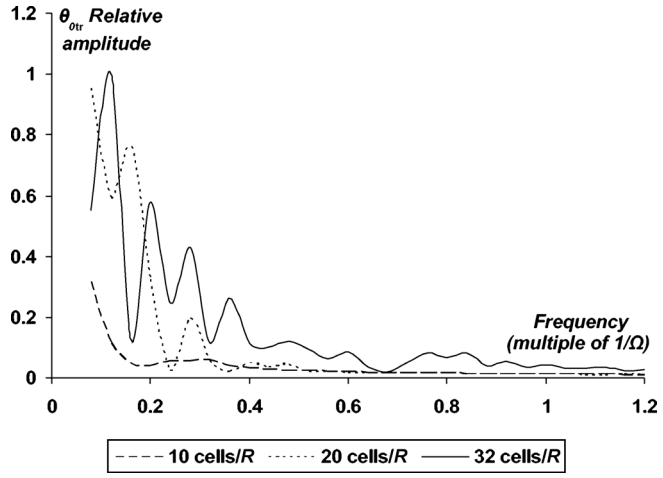

Fig. 2. Sensitivity of tail rotor control response to grid resolution.

flight case, described later in this paper, was used in these tests as it was found that this flight condition resulted in significant fluctuations in the tail rotor collective pitch required to maintain yaw moment equilibrium of the system. The figure shows that a certain minimum resolution of the aerodynamic features in the wake is required for these low-frequency fluctuations to emerge in the simulation. More importantly, the figure shows the basic observed unsteadiness in the simulated control response of the tail rotor to be captured adequately once the cell size is reduced to about a twentieth of the main rotor radius. For this reason, all calculations presented in this paper were performed at this level of resolution. Increasing the cell density further allows a more accurate representation of the tail rotor control response across a broader range of frequencies, but adds significantly to the computational cost without appearing to add materially to the basic physics of the interaction as described in this paper.

It should be noted that at this grid resolution the diameter of the tail rotor is resolved over only about eight computational cells, and this does place a lower limit on the spatial dimensions of any interactional effects present in the simulation that can be fully resolved on the scale of the tail rotor. For instance, individual blade–vortex interactions at the tail rotor are not well captured at this level of resolution. Small-scale effects such as this would appear as high-frequency loads that would have to be properly resolved for accurate calculations of the acoustic or vibrational consequences of main rotor–tail rotor interactions, for instance, but the results presented here show that, given the characteristics of the controller, it is not really necessary to capture the aerodynamic environment of the tail rotor to the same level of detail in a study of the flight mechanics of main rotor–tail rotor interaction.

The Effects of Aerodynamic Interaction

Comparison of the results of simulations of the coupled main rotor–tail rotor system with the results of separate simulations of each individual rotor shows the aerodynamic interaction between the wakes of the two rotors, when operated in close proximity to each other, to have a significant effect on the loads produced on both rotors. The interaction is characterized in particular by a marked increase in the unsteadiness of the loading on the system. This unsteadiness has important consequences for the flight mechanics and handling qualities of the helicopter. Data for seven different flight conditions are presented in this paper and results for simulations with both possible senses of tail rotor rotation are compared. As well as for hover, results are presented for two different forward flight speeds to determine the influence on the tail rotor performance of the rearward skewing of the main rotor wake, and the possibility, over a range of flight speeds, of direct impingement of the main rotor wake on the tail rotor. Left quartering flight (along a bearing of Red 135°) was also examined to determine the effects on tail rotor performance of the relatively long-range interaction between the tail rotor wake and the developing supervortices in the wake of the main rotor, and of the direct convection of the tail rotor wake toward the main rotor. Left and right sideward flight at constant velocity was also considered. In this case the supervortices formed in the wake of the main rotor do indeed pass very close to the tail rotor and influence very strongly its aerodynamic environment. Finally, results from a simulation of accelerated sideward flight to the left are presented. In this example, the tail rotor is exposed to the possible onset of the vortex ring state over a range of flight speeds, and the possibility is that the behavior of the tail rotor, once having succumbed to the instability of its wake and thus having entered the vortex ring state, might be exacerbated by the proximity of the wake of the main rotor. To allow direct comparison between the various cases, the thrust coefficient of the main rotor was maintained at a nominal value of 0.005 throughout. Again, to aid in their comparison, in all but the intermediate-speed forward flight case, where the advance ratio was 0.16, the overall advance ratio was kept constant at 0.04 and the flight condition was varied simply by flying the helicopter at the appropriate angle of sideslip.

Although the flight condition as well as the sense of rotation of the tail rotor has a strong influence on the actual performance of the system, the following example serves to illustrate the generic features of the interaction between the main and tail rotors before the results from the simulations of this broader series of flight conditions are presented and compared. Figures 3(a)–(d) show snapshots of the flow surrounding the helicopter when operated in hover. The structure of the rotor wakes is visualized in these diagrams by plotting a surface on which the vorticity in the flow surrounding the rotor has uniform magnitude. The selected vorticity magnitude is low enough for the global structure of the wake to be clearly apparent. Figure 3(a) shows the wake of the isolated main rotor, and Fig. 3(b) the wake of the isolated tail rotor. When operated in isolation, both rotors generate a well-developed, cylindrical wake tube that extends some distance into the flow downstream of the rotor before succumbing to the natural instability of the wake tube to perturbations to the helicoidal geometry of its constituent vortex filaments. Figures 3(c) and 3(d) show similar snapshots of the combined wakes of the main rotor and tail rotor when operated together, for the two cases where the tail rotor has TA and TF sense of rotation, respectively. When influenced by the flow field of the main rotor wake, the tail rotor wake undergoes a radical change in its geometry. Instead of streaming out to the port side of the helicopter as in the earlier image, after a very short distance it becomes entrained into the wake structure of the main rotor.

Although the snapshots show the wake structures generated by the two systems with opposing sense of tail rotor rotation to be superficially very similar, this format of presentation does not represent very well the unsteadiness of the process by which the wakes of the two rotors merge. This is done more effectively by decomposing the vorticity in the wake into a mean component and an associated RMS fluctuation about the mean. The mean vorticity distribution is approximated simply as the ensemble average

$$\bar{\omega}(x,t) = \frac{1}{2n+1}\sum_{i=-n}^{n}\omega(x, t + i\ \Delta t) \tag{5}$$

over $2n + 1$ snapshots of the wake structure spaced apart by equal time intervals Δt. The associated RMS field representing the local fluctuations

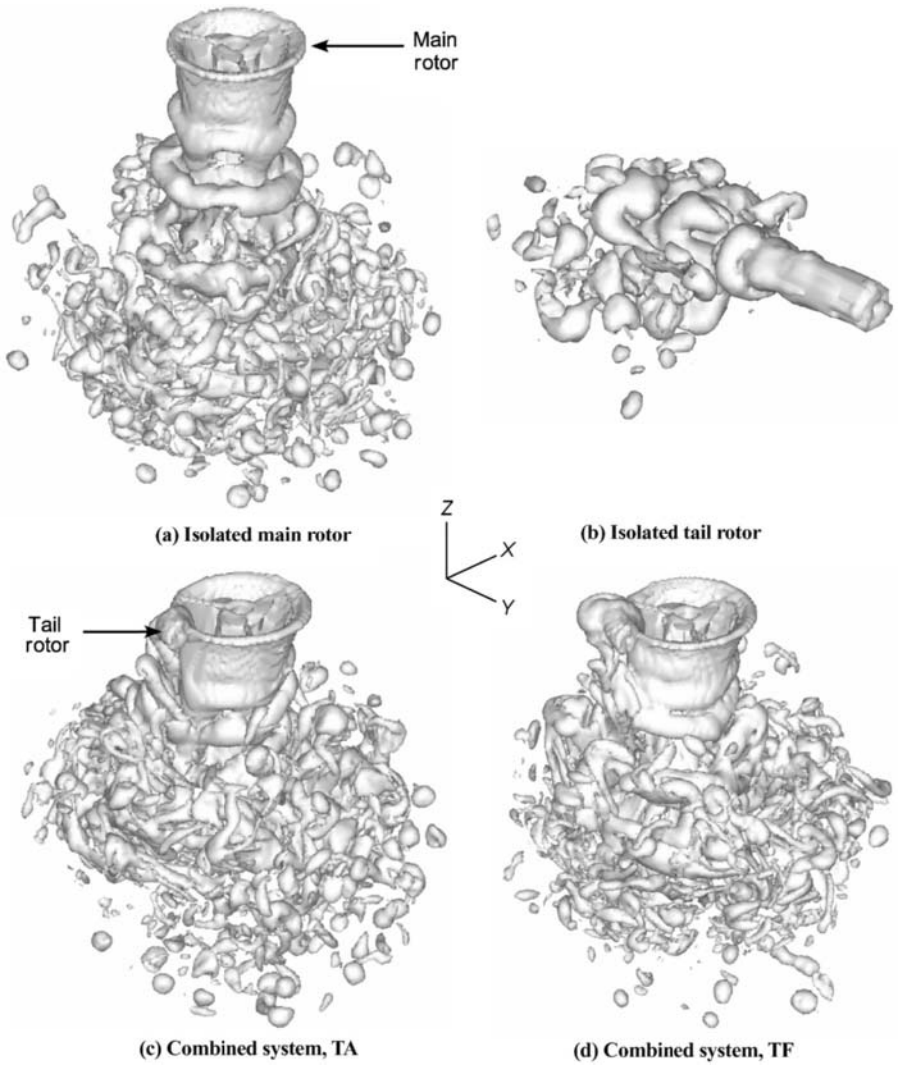

Fig. 3. Instantaneous snapshots of hover wake.

in the wake structure can then be calculated as

$$\hat{\omega}(x,t) = \left[\frac{1}{2n+1} \sum_{i=-n}^{n} (\omega(x, t + i\ \Delta t) - \bar{\omega}(x,t))^2 \right]^{1/2} \tag{6}$$

Figure 4 shows the results of decomposing the flow into a persistent mean component (light, translucent surface) and a fluctuating RMS component (dark surface) using Eqs. (5) and (6). The development of the instability in the wake tube of both the isolated main and tail rotors is exposed very clearly in this form of presentation as a rather sudden increase in the fluctuating component of the vorticity, at the expense of the mean component, some distance downstream of both rotors. The effects of the interaction between the main and tail rotors, both in terms of the distortion of the shape of the mean wake and in the redistribution of the regions of maximum unsteadiness in the wake, are also clearly apparent in the two diagrams showing the flow field of the coupled system.

The systems with opposing directions of tail rotor rotation show not only distinct differences in mean wake geometry, especially in the region affected by the entrainment of the tail rotor wake into the wake-tube of the main rotor, but also in the distribution of the unsteadiness in the flow fields. Interaction with the main rotor wake causes the region of significant unsteadiness in what remains of the distinct wake tube of the tail rotor, if anything, to shrink when the tail rotor rotates TA, and the rather sparse distribution of the fluctuating component of the vorticity in this part of the wake suggests the relative steadiness of the entrainment process in this case. In contrast, when the tail rotor rotates TF, the fluctuating component of the vorticity is strongly concentrated in the region of the confluence of the two wake tubes, indicating that the entrainment process is accompanied by significant variability in the geometry of the wake. The extent to which the wake of the main rotor is affected by the interaction also appears to be quite strongly influenced by the direction of rotation of the tail rotor. With the tail rotor rotating TA, a reasonably narrow tongue of unsteadiness is introduced that extends down from the plane of the main rotor into the flow just to the left of the tail rotor. With the tail rotor rotating in the opposite sense, the region of unsteadiness that is induced in the main rotor wake by the interaction with the tail rotor is much larger, and extends to much of the aft left quadrant of the wake tube.

The positions of these regions of unsteadiness in the flow appear to have a strong, but often quite obscure, influence on the loading produced on the system. It has been found that corresponding high levels of unsteadiness exist in the thrust produced on the tail rotor, for both senses of tail rotor rotation, in several flight conditions. These fluctuations in

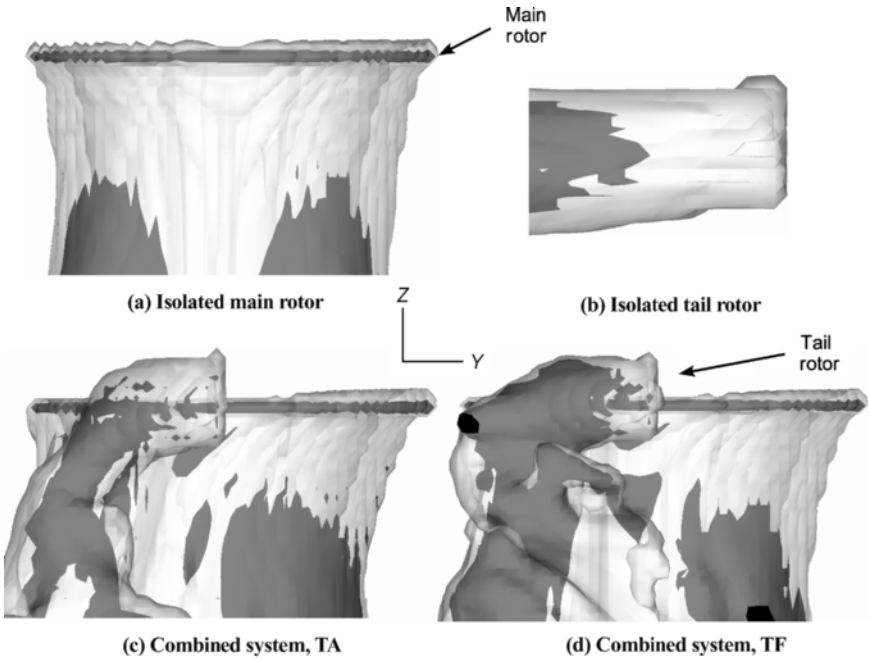

Fig. 4. Decomposition of hover wake into persistent and fluctuating components.

tail rotor thrust yield an unsteady contribution to the yaw moment on the vehicle, as do, in certain flight conditions, similar fluctuations in the torque produced by the main rotor.

Rotor Performance

If the unsteady yaw moment is required to be counteracted by the control system, then the aerodynamic unsteadiness associated with the interaction between the main and tail rotor wakes results in a fluctuation in the tail rotor collective pitch input. Figure 5 shows the actions of the controller in attempting to drive the yaw moment to zero in six of the different flight conditions mentioned earlier, namely hover, level forward flight at low and intermediate speed, left quartering flight, and left and right sideways flight. In each case, data are presented for both senses of tail rotor rotation. The data shown are for a sample extracted far enough into the simulation for the controller to have trimmed the system to a quasi-steady flight condition. In all cases, there appears to be very little obvious periodicity in the control inputs required to trim the helicopter, but their low-frequency character is clearly apparent. It is clear too that the flight condition has a profound effect on the control activity required to maintain the aircraft in trim. Figures 5(b) and 5(d) demonstrate the extent of such activity in quartering and left sideways flight and, to a lesser degree, also in low-speed forward flight as shown in Fig. 5(c). In contrast, little or no variation in tail rotor collective pitch is required to maintain trim in hover and intermediate-speed forward flight, as shown in Figs. 5(a) and 5(e). Most interesting though is that in right sideways flight, as shown in Fig. 5(f), significantly less control activity is required to maintain trim than in the equivalent left sideways flight condition.

A very effective representation of the resultant loading fluctuations on the system is obtained by sampling the data at a fixed frequency (in this paper, unless otherwise stated, at once per main rotor revolution to expose the low-frequency unsteadiness in the signal that is of most relevance to the handling qualities of the aircraft) and projecting the sampled data back onto the real line to suppress the time axis. This representation of the data can be extended to multiple, concurrent time series simply by increasing the number of axes in the plot. A series of such "return maps," comparing the yaw moment contributions from the main and tail rotors, is shown in Fig. 6 for the various flight cases considered in this paper. The scatter of points along each axis provides a measure of the variability in the associated time series, whereas clusters of points sometimes provide evidence of periodicity in the signal at subharmonics of the sampling frequency. Obvious structure in the distribution of points on the return map can sometimes be a sign that the system is governed by low-order dynamics, but such an interpretation needs to be made with care since the consequences are profound.

To aid comparison between the different flight cases, the horizontal and vertical axes in Fig. 6 have both been scaled to represent the ratio of the fluctuation in the yaw moment contribution of each rotor to the mean value of the yaw moment developed by the main rotor in hover at the same thrust coefficient. The diagonal line on the diagrams thus represents the condition in which the net yaw moment on the system is zero. It is clearly evident that the system spends very little time in this condition, and the degree of scatter in the distribution of data points around this line is representative of the magnitude of the fluctuation about equilibrium of the yaw moment on the aircraft. The degree of horizontal scatter of the data compared to the amount of vertical scatter is a measure of the relative contributions of fluctuations in tail rotor thrust and in main rotor torque to the lack of equilibrium within the system.

This form of presentation of the data reveals the main source of interaction-induced unsteady loading in the system to depend quite significantly on the flight condition: in hover and both low-speed and intermediate-speed forward flight, the fluctuations in the thrust produced by the tail rotor are the most significant contributor, suggesting the dominance of the main rotor influence on the tail rotor in driving the interaction between the two rotors in forward flight. Most interestingly, the fluctuations in the tail rotor load are greater in the low-speed case than in the intermediate, suggesting the existence of an intervening advance ratio at which the aerodynamic interaction between the main and tail rotor has the most severe consequences for the handling qualities of the vehicle. The bimodal clustering of points in the return map for the low-speed case is also evidence for the existence of a very low-frequency periodicity in

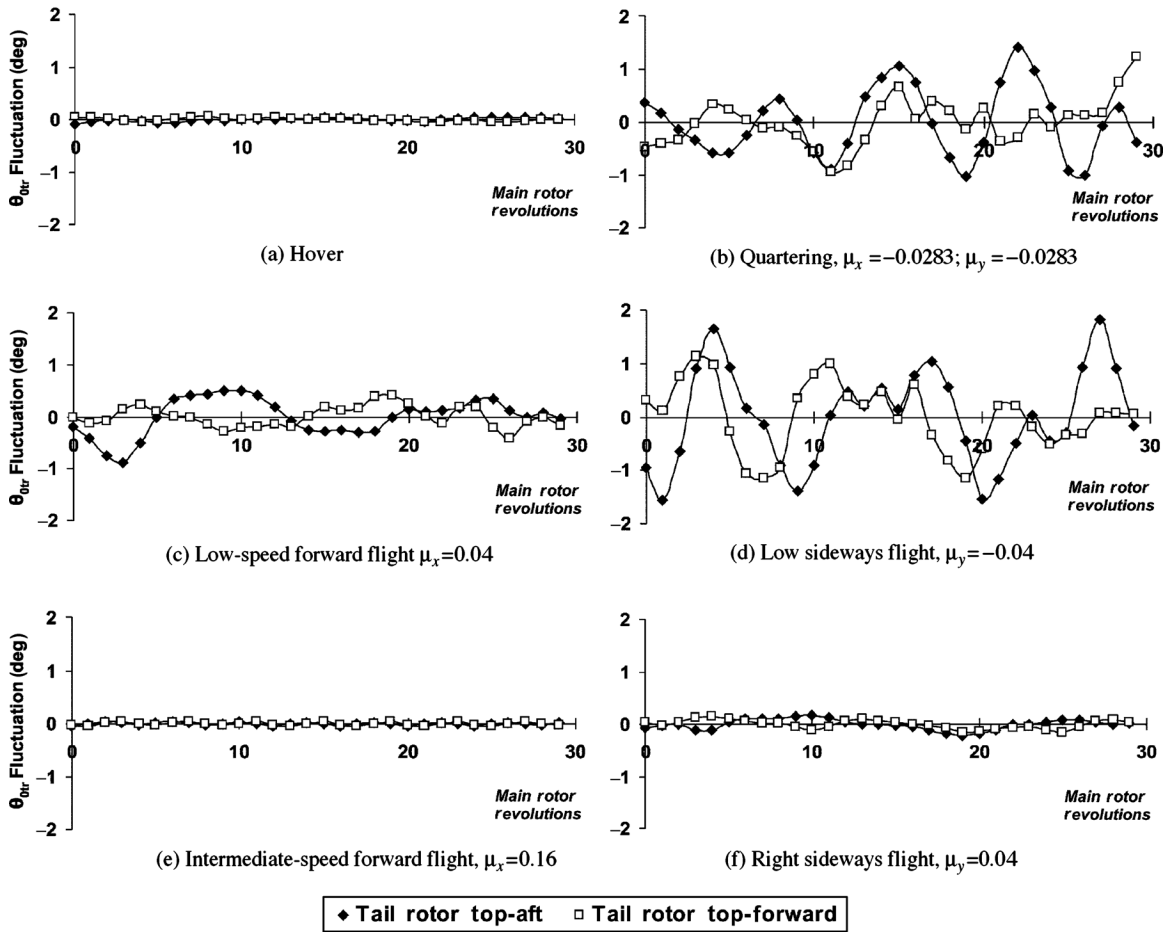

Fig. 5. Variation in tail rotor collective pitch required for trim in yaw.

the forcing of the tail rotor that is not seen in any of the other flight conditions. This periodicity appears to be a slightly more prominent feature of the loading on the system with TF sense of tail rotor rotation than with TA, but besides this feature, the direction of tail rotor rotation appears to have very little influence on the behavior of the system in forward flight.

In quartering and sideways flight, the interaction has a somewhat different character. The fluctuations in yaw moment, although still dominated by the contribution from the tail rotor, arise partially also from the main rotor, suggesting the greater influence of the mutual interaction between the rotors on the dynamics of the system. In sideways flight to the right, both rotors yield relatively moderate contributions to the fluctuating yaw moment on the system, and the behavior of the system is relatively insensitive to the direction of tail rotor rotation. In sideways flight to the left, the system with TF sense of tail rotor rotation shows significantly elevated fluctuations in yaw moment compared to the system with TA-rotating tail rotor, and the contribution to the yaw moment fluctuation from both rotors is significantly more extreme than in sideways flight to the right. The quartering flight case shows a slight elevation in the level of yaw moment fluctuation compared to left sideways flight, and an even greater sensitivity to the direction of tail rotor rotation. Interestingly, the change from TA to TF sense of rotation results in an increase in the yaw moment fluctuations generated by both the main and the tail rotors, rather than, as might be expected if the change in the sense of rotation had a more localized effect on the aerodynamics of the system, just in the yaw moment fluctuation generated by the tail rotor. Despite the rather crude resolution of the aerodynamics of the tail rotor in these simulations, this observation is reasonably strong evidence that the origin of at least part of the sensitivity of the system's dynamics to the sense of rotation of the tail rotor lies in the mutual interference between the wakes generated by the two rotors rather than, as has been suggested in the past, being simply a function of the way that the tail rotor aerodynamic performance is affected by local interaction with the wake of the main rotor (Ref. 18).

In Fig. 7 the statistical distribution of perturbations to the tail rotor yaw moment for an isolated tail rotor and the coupled system in two flight conditions, left quartering flight and pure left sideways flight are represented as a discrete probability density function of perturbation amplitude. It is immediately obvious that the range of amplitudes of disturbance, and the proportion of occurrences at each amplitude, is significantly different for the isolated tail rotor than when coupled with the main rotor. The principal effect of the presence of the main rotor is to reduce the proportion of large excursions in yaw moment generated by the tail rotor. This is strong evidence of a very definite difference in the type of rotor–wake interaction that drives the loading fluctuations on the tail rotor when isolated and when closely coupled with the main rotor.

It is possible that, at the particular advance ratio at which the simulations were conducted, both the left sideways flight case and, to a lesser degree, the quartering flight case may have involved the tail rotor operating in the vortex ring state (VRS). Figure 8 shows the predicted tail rotor collective pitch variation when the aircraft accelerates from hover into left sideways flight. Results from a simulation of the coupled main rotor–tail rotor system where the tail rotor collective pitch was directly controlled to trim the helicopter in yaw (with the tail rotor rotating TA) are compared against a similar simulation of an isolated tail rotor translating through

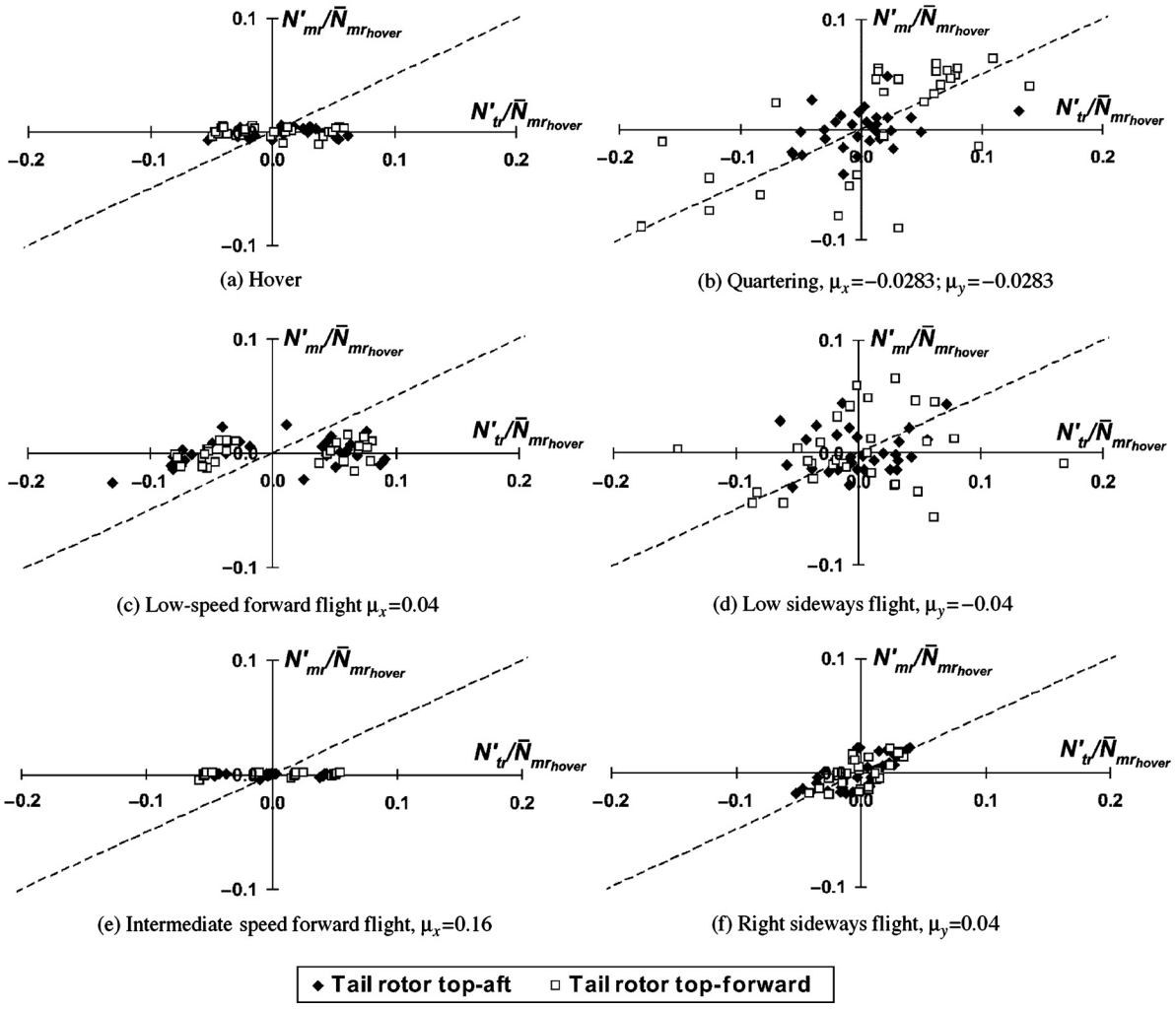

Fig. 6. Main and tail rotor contribution to overall yaw moment on the aircraft.

the same flight trajectory where the tail rotor collective pitch was controlled to counteract the yaw moment developed by the main rotor in the equivalent coupled system. The effect of aerodynamic coupling between the rotors appears to be twofold. First, in the coupled system there is clearly a premature onset of the increase in tail rotor collective pitch with advance ratio required to trim the aircraft. This increase is known to be a characteristic signal of the onset of the vortex ring state in isolated rotors and is required to counteract a loss of thrust on the system associated with the collapse of the wake from its usual cylindrical geometry to a roughly toroidal form. This characteristic thrust settling occurs in a window of advance ratios between 0.02 and 0.04 in the coupled system, but between advance ratios of 0.04 and 0.05 for the isolated tail rotor. The second symptom inherent in the coupled system is a significant increase in the level of unsteadiness in the tail rotor collective pitch throughout the range of advance ratios that were simulated. The qualitative form of both sets of data is supported to some extent by the experimental measurements obtained by Lehman (Ref. 19).

A second horizontal axis has been appended to Fig. 8 to represent the lateral advance ratio of the aircraft scaled by the induced velocity through the tail rotor under hovering conditions, to allow the speed of onset of vortex ring state-like symptoms to be compared to available literature. For instance, the analytic model given by Newman et al. (Ref. 20) provides a reasonably accurate measure of the speed of onset of the VRS for isolated rotors, and would suggest a scaled advance ratio, $\tilde{\mu}_y$, of approximately 0.6; thus an equivalent lateral advance ratio of the helicopter, μ_y, of about 0.035 for the onset of the VRS for the range of thrust coefficients produced by the tail rotor in trimming the aircraft in sideways flight. This value is in reasonable agreement with the isolated rotor data shown in Fig. 8 for the onset of VRS-like behavior at the tail rotor, but is at odds with the predicted onset speed in the coupled system. It was shown earlier that, even in hover, the development of the tail rotor wake is severely disrupted by interaction with the main rotor, and the results presented here thus raise the question of whether it is appropriate to analyze the dynamics of the tail rotor using the possibly oversimplified concepts of isolated rotor VRS, or whether instead a more coherent view, spanning a broader range of flight conditions, is required of the disruption of the tail rotor wake that is brought on in the presence of the main rotor.

Wake Interaction

The information presented in the previous section of this paper suggests that the form of aerodynamic interaction responsible for the observed aerodynamic behavior of the coupled main rotor–tail rotor system may be quite strongly dependent on flight condition. In forward flight, the interaction appears to be dominated by the influence of the main rotor on the tail rotor, whereas the behavior of the loading in flight conditions with some lateral component of velocity seems to be more strongly influenced by the mutual effect of both rotors on each other. Indeed, it is possible

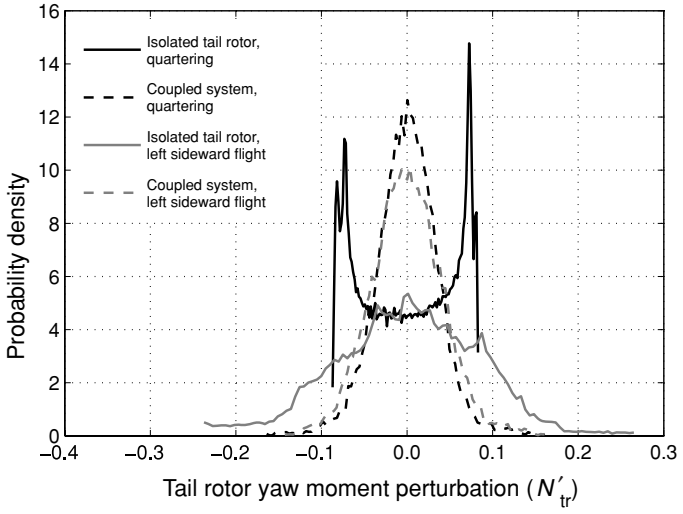

Fig. 7. Representation of tail rotor aerodynamic unsteadiness in quartering and left sideways flight via the statistical distribution of yaw moment perturbations of various sizes.

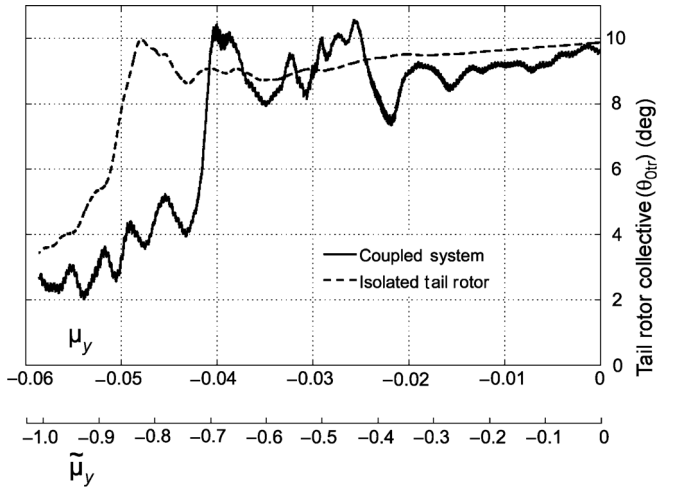

Fig. 8. Variation of tail rotor collective pitch with sideways velocity in accelerated sideways flight.

to imagine two rather different modes of aerodynamic interaction taking place within the system. The first, rather obvious "direct" mode would involve the direct impingement of the wake of one of the rotors on the other rotor, and thus a direct and strong modification of the aerodynamic environment experienced by the blades and hence the performance of the affected rotor. The second "indirect" mode, where interaction between the wakes of the rotors–perhaps even at quite some distance from the rotors themselves–modifies the geometry of both wakes, and thus feeds back into the aerodynamic environment of the system and hence the loading on the rotors in a far more subtle way than in the first case, has not received much attention in the past.

The possible existence of the direct mode of interaction can be reasonably clearly inferred from an examination of the mean geometry of the wake, whereas the existence of the second, indirect mode requires a somewhat more tenuous extrapolation from an analysis of local fluctuations in the strength of the wake to determine the locations of the regions of maximum aerodynamic unsteadiness in the system. Figures 9 and 10 show the wakes generated by the system under the various flight conditions discussed previously. In each figure, the diagrams at left show illustrative snapshots of the wake structure at one particular instant during its evolution while the figures in the center and to the right show the wake decomposed into a steady, mean component (light, translucent surface) and a fluctuating component (dark surface) by applying the analysis presented in the section "The Effects of Aerodynamic Interaction" to simulated wake data collected over several rotor revolutions. It should be noted that the appearance of the main rotor blades in the RMS component of the wake is simply a strobing effect that is induced by the finite frequency at which the vorticity field was sampled.

Comparison of Figs. 3, 11, and 9 reveals the changes in wake structure as the forward speed of the helicopter is increased. Since the tip speed for both main and tail rotors is very similar for the configuration tested here, the wakes of both rotors in isolation behave very similarly at the same forward speed. As the advance ratio of the system is increased, the cylindrical, hover-like wake of the isolated rotor skews back and the vorticity begins to roll up shortly behind the rotor disk, eventually to form a pair of concentrated, counterrotating supervortices along either side of the wake. At an advance ratio of about 0.1, the wake of an isolated rotor undergoes a transition from the tubular form found at lower advance ratio to a flattened, more aeroplane-like form. As the forward speed of the rotor is increased, the structure of the wake becomes more pronounced, and the point of visible disruption of the wake as a result of the inherent instability of its vortical structure moves further and further downstream of the rotor. This isolated rotor-like behavior is still evident in the geometries of the wakes of the coupled main rotor–tail rotor system. For instance, the transition in the form of the wakes of both main and tail rotors is very clear when comparing the flow fields shown in Figs. 11 ($\mu = 0.16$) and 9(a) ($\mu = 0.04$). The situation is complicated though by the increasing impingement of the main rotor wake on the tail rotor as the forward speed is increased. In the low-speed forward flight case, although roughly the bottom quarter of the tail rotor is immersed in the wake of the main rotor, the tail rotor wake maintains its tubular form for quite some distance before gradually merging with the main rotor wake some 3–4 main rotor radii downstream of the rotors. In the intermediate-speed forward flight case, whilst the entire lower half of the tail rotor is immersed in the wake of the main rotor, the distinct character of the tail rotor wake is visible as the spine-like feature that persists for well over 12 main rotor radii down the center of the wake of the combined system.

It was shown earlier that of the two forward flight cases, the greatest fluctuations in the performance of the system were to be found in the low-speed forward flight case. The degree of direct impingement of the main rotor wake on the tail rotor cannot thus be the prime factor in governing the low-frequency unsteadiness in the forces produced by the system. Figure 9(b), showing the decomposition of the wake into persistent and fluctuating components in low-speed forward flight, unsurprisingly shows a significant zone of unsteadiness around where the main rotor wake impinges on the tail rotor. This unsteadiness is, in all likelihood, directly responsible for the unsteadiness in the loads generated by the tail rotor. Importantly though, the unsteadiness in the wake also extends outward in a crescent-shaped arc along the trajectory followed by the lower supervortex from the tail rotor as it merges into the wake of the main rotor. Comparison of Fig. 9(b) with Fig. 9(e) demonstrates that the shape of this arc is subtly dependent on the direction of tail rotor rotation. This distribution of unsteadiness is directly associated with the interaction of the main and tail rotors and the amalgamation of their respective induced wakes since it does not exist in the wake of the isolated main rotor under the same flight conditions as shown from two different perspectives in Figs. 9(c) and 9(h). Instead, smaller, tubular regions of unsteadiness appear which are associated with vortex dynamics during the creation of the main rotor's supervortices. The secondary region of strong unsteadiness in the supervortex on the advancing side of the main

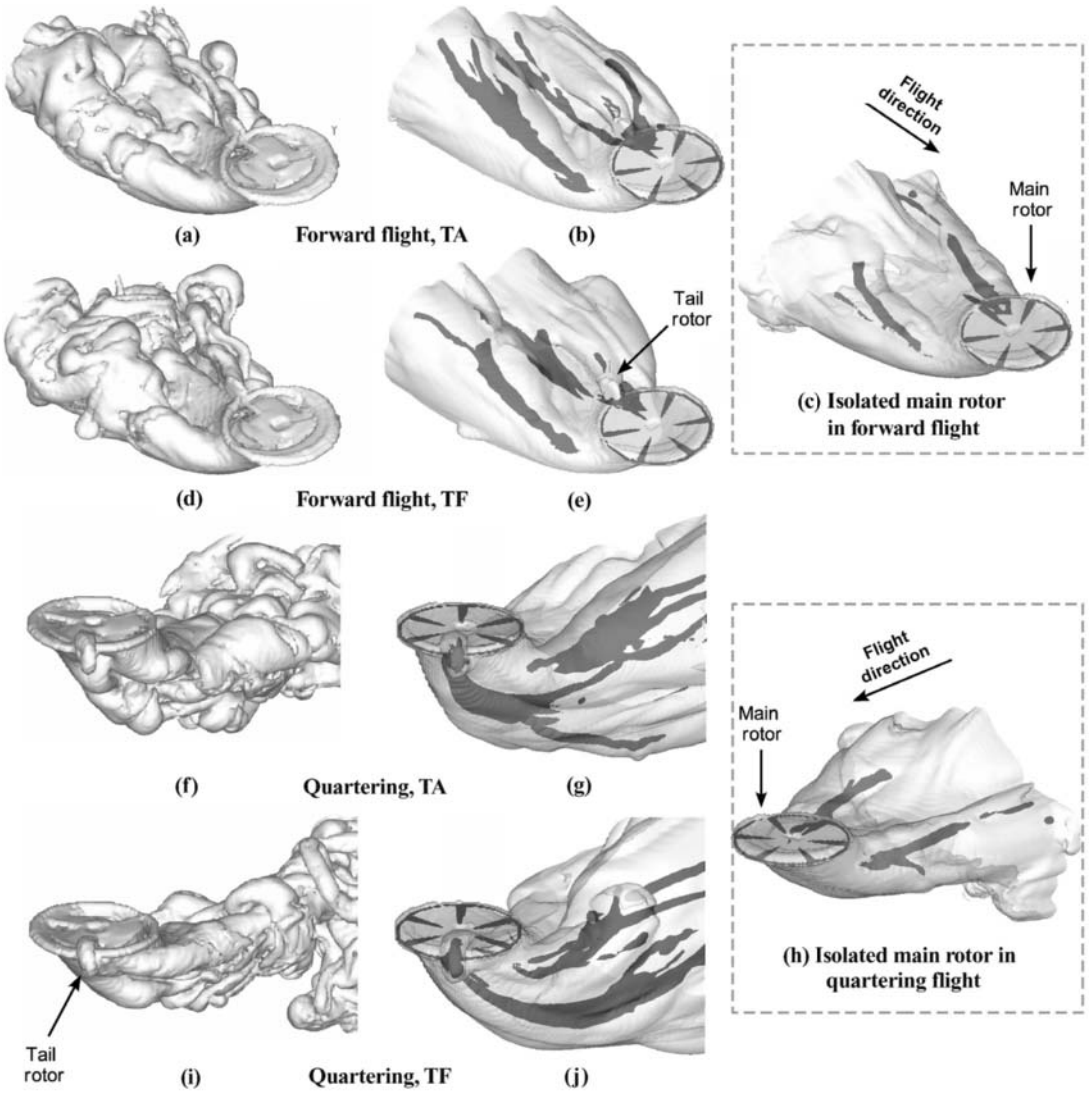

Fig. 9. Wake structure in various flight conditions; left: instantaneous, center and right: mean and RMS.

rotor wake in this flight condition is largely unaffected by the interaction between the two rotors, but the observed enlargement of the region of excitation within the retreating side supervortex through interaction with the tail rotor wake may be partially responsible for indirectly forcing the rather weak unsteadiness in the loading on the main rotor that is observed in this flight condition.

In the quartering flight case, the tail rotor is located upwind of the main rotor, and the free stream thus aids in the tail rotor wake being entrained almost directly into the main rotor where it causes significant disruption to the development of the leading edge of the main rotor wake. This disruption is clearly evident in the snapshots presented in Figs. 9(f) and 9(i) and appears in the associated decompositions of the wake structure (Figs. 9(g) and 9(j)) as a distinct concentration of the variability in the wake structure down the forward surface of the wake that extends well into the flow downstream of the system; a feature that is clearly not evident in the wake of the isolated main rotor (Fig. 9(h)). The vorticity distribution surrounding the tail rotor is also highly variable, but, comparing snapshots, the stream of vorticity produced by this rotor appears to be more coherent in structure than in left sideways flight. The direction of rotation of the tail rotor appears to have a rather subtle influence on the distribution of unsteadiness in the wake, but, rather surprisingly, a marked influence on the geometry of the mean wake of the system. A comparison of Figs. 9(g) and 9(j) shows the mean wake of the system with TA tail rotor rotation to be broader and flatter than the wake of the system with tail rotor rotating TF, and this appears to be associated, in, admittedly, a rather obscure way, with the induction of the tail rotor wake into the supervortex on the closest side of the main rotor disk. The principal effect of tail rotor rotation in this flight condition may thus be to promote an indirect mode of interaction between the rotors by raising the fluctuating vorticity field embedded within this supervortex closer to the main rotor disk, where it can have a greater effect on the unsteadiness of the loads produced by the system.

It is highly instructive to compare the wake geometries generated by the rotors in left sideward and right sideward flight. In right sideward flight (Figs. 10(f)–10(g) and 10(i)–10(j)), the effect of the free stream in having a significant component in the direction of the induced velocity of the tail rotor is to prevent the wake tube produced by the tail rotor from being entrained through the main rotor. Instead, the wake tube remains relatively intact as it extends a considerable distance downstream, parallel to the supervortex on the same side of the main rotor disk. The induced velocity field of the supervortex gradually flattens the tail rotor wake tube and bends it slightly inward toward the centerline of the main rotor wake,

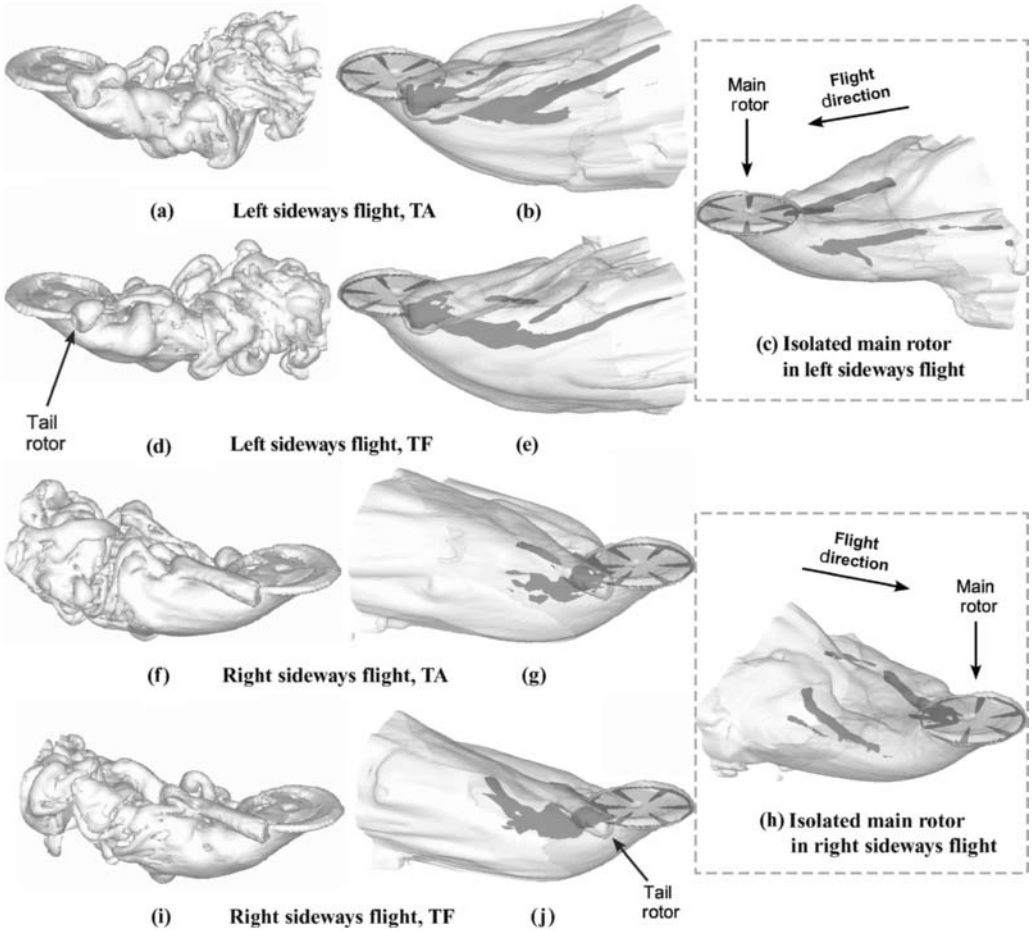

Fig. 10. Wake structure in various flight conditions; left: instantaneous, center and right: mean and RMS.

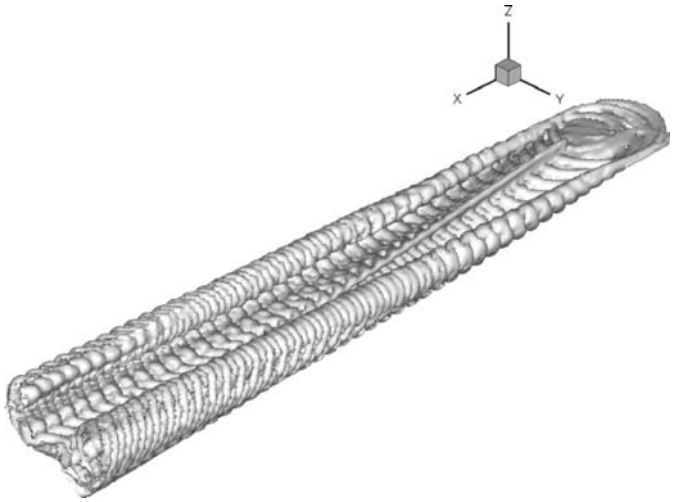

Fig. 11. Wake of a combined rotor system in intermediate-speed forward flight; tail rotor top-aft.

and eventually the two wakes merge within the highly disrupted flow well downstream of the rotors. This fairly ordered structure produces very isolated and small regions of fluctuation in the wake, consistently with the low levels of fluctuating load observed under this flight condition. In contrast, the left sideward flight case (Figs. 10(a)–10(b) and 10(d)–10(e)) is much more interesting since the free stream velocity, now in opposition to the induced velocity of the tail rotor, prevents the tail rotor wake from advancing very far downstream. Instead, it is drawn toward the main rotor, and parts of the tail rotor wake tube are subsequently entrained into the main rotor wake in a highly unsteady process that extends back to the tail rotor disk. This wake dynamics is most likely to be the direct cause of the fluctuations in loading observed on the tail rotor. Those remnants of the tail rotor wake that are not ingested into the main rotor are emitted in highly disrupted form as a stream of fragments that are convected back into the wake behind the system along a trajectory that is almost the mirror image of that of the tail rotor wake in right sideward flight. As in right sideward flight, the induced velocity field of the supervortex on the closest side of the main rotor flattens this stream of vorticity and rotates it inboard causing it to interact rather strongly with the periphery of the main rotor near the point of formation of the supervortex. Given the highly unsteady nature of the stream of vorticity emanating from the tail rotor, this interaction has a significant effect in increasing the unsteadiness of the flow in the supervortex itself, and the presence of this indirect mode of interaction is the most likely cause of the substantially increased unsteadiness in the loading produced by the main rotor in left sideward flight compared to right sideward flight. The effect of tail rotor sense of rotation is not immediately obvious, however, since Figs. 10(b) and 10(e) show a change in direction of rotation of the tail rotor to be accompanied by no gross changes in the structure of the mean wake, and only subtle shifts in location of the regions of major unsteadiness within the flow field of the system.

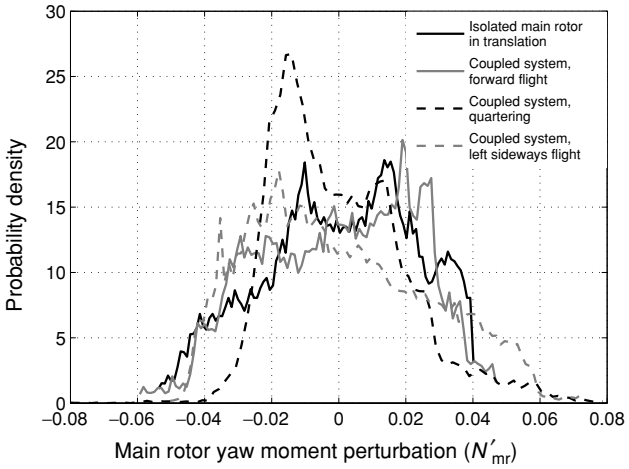

Fig. 12. Representation of main rotor aerodynamic unsteadiness in various flight conditions via the statistical distribution of yaw moment perturbations of various sizes.

Figure 12 represents the magnitude of the fluctuations in the main rotor contribution to the yaw moment on the aircraft as a discrete probability density function (PDF). The increased proportion of small-amplitude fluctuations in the main rotor torque in quartering flight is caused by a disruption to the loading near the tips of the main rotor blades as they pass across the rear half of the main rotor disk. This disruption is almost certainly associated with the flow distortions that are induced by the entrainment of the wake of the tail rotor through the main rotor in this flight condition. The torque generated by the main rotor in the other flight conditions represented in the figure, where direct impingement of the tail rotor wake on the main rotor is not a strong feature of the interaction between the two rotors, does not exhibit the same characteristic elevation of activity in this part of the PDF, yet still exhibits a significant degree of unsteadiness. This is highly suggestive of the existence of the two distinct modes of interaction between the rotors that was postulated earlier.

Returning to the question of whether or not the tail rotor exhibits vortex ring-like behavior in left sideways and quartering flight, comparison of Figs. 10(a) and 9(f) (the hover wake shown in Fig. 3 can be included as a useful intermediate case) shows that the behavior of the flow near the tail rotor in lateral flight exhibits a somewhat more complex mechanism of VRS onset than is the case with an isolated rotor. The breakdown of the cylindrical wake tube into a toroidal form over a small range of free stream velocities that oppose the induced flow through the rotor is significantly less abrupt in the case of the coupled-rotor system. The simulations suggest that the tail rotor wake is highly disrupted in all lateral flight conditions by its entrainment into the wake of the main rotor. Indeed, the principal mode of behavior of the tail rotor wake, in response to a change in the component of the free stream that is parallel to its axis, appears simply to be a lengthening or shortening of the segment of the wake tube that is left relatively undisturbed by this entrainment. The reason why the response of the rotor does appear to have a vortex ring-like character at the highest opposing free stream velocities can be inferred with reasonable confidence from the figures: under these conditions the undisturbed segment of the wake does indeed become very short, and the tail rotor itself thus becomes immersed in the highly unsteady vorticity field associated with the entrainment of the tail rotor vorticity into the wake of the main rotor. Thus, the wake of the combined system does indeed bear some of the hallmarks of the flow field generated by an isolated rotor immersed in the classical VRS (as confirmed by Fig. 8), and it is not surprising that the tail rotor exhibits similar performance characteristics under these conditions.

Implications for Helicopter Directional Control

To place the data presented in this paper in perspective, it is useful to consider that 1° of tail rotor collective pitch input would require roughly 6–7% of the pedal travel available to the pilot on a typical helicopter. This implies that the 3° or so maximum variation in collective pitch observed in the worst cases presented in Fig. 5 would correspond to pedal motion over roughly 20% of the available range. Furthermore, the data presented in Fig. 5 show that the largest amplitude variations in tail rotor collective pitch would be required to be made with a characteristic period of roughly 5–10 main rotor revolutions. For a typical helicopter, where the main rotor might rotate at a frequency of 4–5 Hz, the largest control applications would thus be required at a frequency in the range of 0.5–1 Hz. This combination of amplitude and frequency of pedal input would arguably be manageable, but nevertheless extremely distracting and tiresome for the pilot under even the most benign operational conditions. Note too that if the pilot were tempted to remain passive rather than to actively apply the requisite control inputs to trim the aircraft, excitation of the system in the 0.5–1 Hz frequency range would stimulate the yaw dynamics of the airframe, quite possibly resulting in a rather objectionable lateral oscillation of the system.

In applying the results presented in this paper to the real situation, however, the implications of some of the simplifications that were embodied in the analysis, here simply for the purposes of better understanding the aerodynamic effects that govern the interaction between the main and tail rotors, should be borne firmly in mind. Whilst the yaw dynamics of the helicopter may indeed be excited by fluctuations in the yaw moment produced by the rotors, as observed here, the role of the fuselage, tail boom, and empennage in acting as strong modifiers to the dynamics of the isolated rotors needs also to be considered. Although the main and tail rotors might be the principal sources of the forces and moments exerted on the helicopter, the loads developed on the fuselage and fin can also be significant. Their contributions to the yaw moment of the aircraft, both as a result of sideslip and yaw rate, may be expected to modify quite strongly the control inputs required at the tail rotor to maintain the yaw equilibrium of the system in any particular flight condition. A lateral dynamic that is suppressed by the very changes to the forces and moments on the helicopter that it induces may be of little consequence to the handling qualities of the vehicle. Conversely, though, one that leads to a divergence in yaw attitude may be highly problematic. Further insight here will require the use of a model that is capable of capturing both the yawing motion of the airframe and the dynamic nature of the resultant flow field that surrounds the helicopter. Of course, the fuselage, empennage, and other components of the airframe act themselves to modify the aerodynamic environment experienced by the rotors. As such, the aerodynamic mechanisms postulated here as the underlying factors governing the interaction between the main and tail rotors may be overwhelmed, in certain cases, by certain configuration-specific elements of the flow field. In such conditions, one may only conjecture as to the specific characteristics of the lateral response of the aircraft, and a generic analysis such as presented here may not be of much specific use. It is particularly these configuration-specific issues that will provide industrial CFD practitioners with a rich source of employment for many years to come, but it is hoped that more general analyses such as the one presented here will be of assistance in providing the fundamental framework within which the more case-specific features of the aerodynamic interaction between the main and tail rotor of any particular configuration can be analyzed and understood.

Conclusion

Simulations of an idealized helicopter, consisting of a main and tail rotor arranged in conventional configuration, have been performed in a range of flight conditions including hover, low-speed, and intermediate-speed forward flight, and three conditions with a lateral component of velocity. The helicopter was modeled as an isolated pair of rotors to avoid other physical factors from obscuring the effects of the aerodynamic interaction between the wakes of the two rotors on the loads produced within the system. Previous studies have suggested that the flight condition as well as the direction of tail rotor rotation (top-forward or top-aft) has a significant effect, particularly on the unsteadiness of the forces produced by the tail rotor. The numerical data presented in this paper support these observations, and the detailed flow field information that is available from the simulations allows some insight into the aerodynamic effects that are responsible for the unsteadiness in the system.

In particular, simulations show distinct differences in the behavior of the system in left sideward and right sideward flight that are consistent with flight experience that the greatest fluctuations in loading or control input are required in left sideways flight (for a counterclockwise rotating main rotor) and are generally more extreme for a system with tail rotor rotating top-forward than top-aft. The simulations also expose distinct differences in the character of the lateral excitation of the system as forward flight speed is varied, and suggest the existence of an intermediate flight speed at which the lateral dynamics of the system is most strongly affected by fluctuations in the loads on the system. Traces of very low-frequency periodicity in the simulated results at low forward speed may be evidence that main rotor–tail rotor interaction might be partially responsible for such practically encountered lateral oscillations such as tail shake or lateral snaking but further investigation, involving significantly longer computational runs than attempted here, is warranted before definite conclusions can be drawn.

The key aerodynamic factor that helps to explain all the cases presented here, though, appears to be the fact that the tail rotor wake undergoes a distinct change in geometry when exposed to the flow field of the main rotor. Instead of streaming out laterally as a coherent tube, as it would in isolation from the main rotor, the wake is disrupted downstream of the tail rotor by a process whereby some or all of its vorticity is entrained into the wake of the main rotor. This entrainment is in all cases a highly unsteady process, and the degree of unsteadiness appears to depend, to some extent, on the direction of rotation of the tail rotor. The disruption to rotor loading appears to be strongly linked to the proximity of the major regions of entrainment-related unsteadiness in the combined wake of the main rotor–tail rotor system to the rotor in question. In intermediate-speed forward flight and right sideward flight, the free stream acts to delay the entrainment to far enough downstream of the system for the perturbations to the rotor loading to be slight. Conversely though, in left sideward and quartering flight, the action of the free stream is to confine the entrainment process very close to the rotors where it has a major effect on the unsteadiness of the loads produced by the system.

As is often the case in complex flow environments, the direct link between cause and effect remains tenuous, and in some cases even elusive. Much further work needs to be done to understand the detailed effects of the aerodynamic interactions that occur in the flow around the closely coupled main rotor–tail rotor geometry of the conventional helicopter configuration on the loads that are produced. Nevertheless, the results of the case study presented here demonstrate that current computational models are indeed sensitive to important operational factors, such as the flight condition of the helicopter, as well as to the more detailed, specific features of the helicopter configuration such as the direction of rotation of the tail rotor that are known to influence the interactional aerodynamic environment of the helicopter. This bodes well for our future understanding of the extremely complex aerodynamics that underlies the performance of the various closely coupled components of the helicopter system.

Acknowledgments

The research reported in this paper has been made possible through the support and sponsorship of the U.S. Government through its European Research Office of the U.S. Army.

References

[1]Sheridan, P. F., and Smith, R. P., "Interactional Aerodynamics—A New Challenge to Helicopter Technology," *Journal of the American Helicopter Society*, Vol. 25, (1), 1980, pp. 3–21.

[2]Lynn, R. R., Robinson, F. D., Batra, N. N., and Duhon, J. M., "Tail Rotor Design Part 1: Aerodynamics," *Journal of the American Helicopter Society*, Vol. 15, (4), 1970, pp. 2–15.

[3]Johnston, J. F., and Cook, J. R., "AH-56A Vehicle Development," American Helicopter Society 27th Annual National V/STOL Forum, Washington, DC, May 4–6, 1971.

[4]Amer, K. B., Prouty, R. W., Walton, R. P., and Engle, J. E., "Handling Qualities of Army/Hughes YAH-64 Advanced Attack Helicopter," Preprint no. 78-31, American Helicopter Society 34th Annual National Forum, Washington, DC, May 15–17, 1978, pp. 78.31.1–78.31.17.

[5]Prouty, R. W., *Helicopter Performance, Stability, and Control*, Krieger, Malabar, FL, 1986, pp. 107–111.

[6]Yeager, W. T., Jr., Young, W. H., Jr., and Mantay, W. R., "A Wind-Tunnel Investigation of Parameters Affecting Helicopter Directional Control at Low Speeds in Ground Effect," NACA TN D-7694, 1974.

[7]de Waard, P., and Trouvé, M., "Tail Shake Vibration in Flight: Objective Comparison of Aerodynamic Configurations in a Subjective Environment," AHS International 55th Annual Forum Proceedings, Montreal, Canada, May 25–27, 1999.

[8]Balch, D. T., "Experimental Study of Main Rotor/Tail Rotor/Airframe Interaction in Hover," American Helicopter Society 39th Annual Forum Proceedings, St. Louis, MO, May 9–11, 1983.

[9]Empey, R. W., and Ormiston, R. A., "Tail-Rotor Thrust on a 5.5-Foot Helicopter Model in Ground Effect," American Helicopter Society 30th Annual National Forum, Washington, DC, May 7–9, 1974.

[10]Wiesner, W., and Kohler, G., "Tail Rotor Performance in Presence of Main Rotor, Ground, and Winds," *Journal of the American Helicopter Society*, Vol. 19, (3), 1974, pp. 2–9.

[11]Brown, R. E., "Rotor Wake Modelling for Flight Dynamic Simulation of Helicopters," *AIAA Journal*, Vol. 38, (1), 2000, pp. 57–63.

[12]Brown, R. E., and Line, A. J., "Efficient High-Resolution Wake Modelling Using the Vorticity Transport Equation," *AIAA Journal*, Vol. 43, (7), 2005, pp. 1434–1443.

[13]Toro, E. F, "A Weighted Average Flux Method for Hyperbolic Conservation Laws," *Proceedings of the Royal Society of London, Series A: Mathematical and Physical Sciences*, Vol. 423, (1864), 1989, pp. 401–418.

[14]Brown, R. E., and Houston, S. S., "Comparison of Induced Velocity Models for Helicopter Flight Mechanics," *Journal of Aircraft*, Vol. 37, (4), 2000, pp. 623–629.

[15]Houston, S. S., and Brown, R. E., "Rotor-Wake Modeling for Simulation of Helicopter Flight Mechanics in Autorotation," *Journal of Aircraft*, Vol. 40, (5), 2003, pp. 938–945.

[16]Whitehouse, G. R., and Brown, R. E., "Modeling the Mutual Distortions of Interacting Helicopter and Aircraft Wakes," *Journal of Aircraft*, Vol. 40, (3), 2003, pp. 440–449.

[17]Ahlin, G. A., and Brown, R. E., "The Vortex Dynamics of the Rotor Vortex Ring Phenomenon," American Helicopter Society 63rd Annual Forum Proceedings, Virginia Beach, VA, May 1–3, 2007.

[18]Ellin, A. D. S., "Lynx Main Rotor/Tail Rotor Interactions: Mechanisms and Modelling," *Proceedings of the Institution of Mechanical Engineers, Part G, Journal of Aerospace Engineering*, Vol. 208, (G2), 1994, pp. 115–128.

[19]Lehman, A. F., "Model Studies of Helicopter Tail Rotor Flow Patterns in and Out of Ground Effect," USAAVLABS TR 71–12, 1971.

[20]Newman, S. J., Brown, R., Perry, F. J., Lewis, S., Orchard, M., and Mohda, A., "Predicting the Onset of Wake Breakdown for Rotors in Descending Flight," *Journal of the American Helicopter Society*, Vol. 48, (1), 2003, pp. 28–38.